# The correlation between ZDDP tribofilm morphology and the microstructure of steel

J. Jelita Rydel[a,*], K. Pagkalis[b], A. Kadiric[b], P.E.J. Rivera-Díaz-del-Castillo[a]

[a] *SKF University Technology Centre, Department of Materials Science and Metallurgy, University of Cambridge, 27 Charles Babbage Rd., Cambridge, CB3 0FS, United Kingdom*

[b] *SKF University Technology Centre, Tribology Group, Department of Mechanical Engineering, Imperial College, South Kensington Campus, London, SW7 2AZ, United Kingdom*

**Abstract**

The microstructure of most hard steels used in tribological applications is inhomogeneous at a micro-scale. This results in local variations in chemical composition and mechanical properties. On a similar scale, tribofilms formed by ZDDP and other anti-wear additives are commonly observed to exhibit a patch-like morphology. ZDDP tribofilms formed under controlled contact conditions on four different steel grades were carefully studied with a new AFM technique to analyse the relationship between the steel microstructure and the tribofilm morphology. Tribofilms were found to be thinner on residual carbides than on the martensitic matrix in all grades containing residual carbides. In most cases, the difference in tribofilm thickness is larger than the carbide protrusion.

*Keywords:* Tribochemistry, Lubricant additives, Surface structure, Atomic force microscopy

*Corresponding author

*Email addresses:* jj393@cam.ac.uk (J. Jelita Rydel), k.pagkalis13@imperial.ac.uk (K. Pagkalis), a.kadiric@imperial.ac.uk (A. Kadiric), pejr2@cam.ac.uk (P.E.J. Rivera-Díaz-del-Castillo)

## 1. Introduction

As a result of high loads, low rotational speeds and low oil viscosities, many tribological contacts operate in boundary or mixed lubrication regimes. Such conditions imply that at least part of the load is supported by direct mechanical interaction between asperities, which may result in surface damage. To prevent early failure due to wear-related surface deterioration in such contacts, special chemicals forming surface protective layers are blended into lubricants. The most common of these are anti-wear (AW) additives.

Zinc dialkyl dithiophosphates (ZDDPs) are the most popular representatives of this group of additives, due to excellent AW performance and a relatively low cost, as well as some additional beneficial properties such as their extreme-pressure (EP) and anti-oxidant functionalities [1, 2, 3]. As an alternative to ZDDPs, ashless phosphorus-containing AW additives are often employed in applications where the ZDDP content has to be limited due to environmental concerns [4, 5]. In tribochemical tests ZDDP is known to form tribofilms that on the micro-scale exhibit a patch-like morphology [1, 6, 7, 8]. Tribofilms developed by ashless AW additives in some cases exhibit resemblance to those formed by ZDDPs and patch-like structures are also sometimes observed [9, 10, 4]. Such patchiness is generally undesirable since it significantly increases surface roughness, especially for initially smooth surfaces [11, 12, 13, 14, 15, 1, 16, 17, 18, 19] and consequently leads to higher asperity stresses with the associated risk of surface damage.

AW additives have been observed to cause an increase in coefficient of friction in mixed lubrication regime [5, 20, 17, 16]. This was initially thought to be related to increased surface roughness and tribofilm directionality [5, 17], although more detailed studies performed by Spikes and Taylor [16, 21] suggest that effects other than surface roughness may also play a role in the mechanism through which ZDDP increases the coefficient of friction.

As the formation of AW films is tribologically triggered, some researchers have attributed the morphology of anti-wear tribofilms to asperities present initially on tested specimens with preferential tribofilm formation in such regions resulting from increased local contact pressure [22, 23, 7].

On the other hand, AW additives interact with the steel surface either by adsorption or chemical reaction to form the tribofilm [24, 25] and therefore it is feasible that microscopic variations in the substrate material composition could influence the film growth locally, which would contribute to the reported uneven coverage of the surface. The microstructure of most hard

steels used in tribological applications, such as bearing and gear steels, is highly inhomogeneous and consist not only of a martensitic or bainitic matrix, but also of other phases with distinctive chemical composition, crystallographic structure and mechanical properties, such as residual carbides, retained austenite and non-metallic inclusions [26, 27, 28, 29]. Two of these microstructural constituents, namely residual carbides and retained austenite, often exhibit sizes very similar to tribofilm islands. Recent investigations [30, 12] show that the thickness of the tribofilm and its evolution depends not only on the tribological conditions, but also on the steel grade that is used for testing. Therefore, micro-scale variations in chemical composition may also be expected to affect the tribofilm thickness on a similar scale.

It has been shown that for Al-Si based alloys, which consist of Al- and Si-rich phases, under certain conditions tribofilm is preferentially formed on harder Si-rich phases in contrast to softer Al-rich phases [31]. In a study of ZDDP-derived tribofilm on an Al-Si alloy performed with the use of various chemical micro-analysis techniques, Nicholls *et al.* [31] attributed this effect to the increased contact pressure, to which Si-rich precipitates are exposed, as these were shown to protrude by about 150 nm from the Al-rich matrix. Xia *et al.* [32] have noted that when oil containing ZDDP and a low concentration of molybdenum dialkyldithiocarbamate (MoDTC) is used to lubricate Al-Si alloy - cast iron tribocouples, it results in more pronounced wear of the Al-matrix with respect to hard Si-rich phase. The tribofilm is then preferentially formed on protruding Si-rich precipitates, which remain in contact with the counterface. Other tribological behaviours were observed by Xia *et al.* [32] when oils containing only ZDDP or ZDDP and high concentration of MoDTC were used.

Although the tribofilm formation on Al-Si based alloys has been shown to be associated with microstructure of the material and it is well known that the microstructure of typical hard steels used in tribological applications, is also highly inhomogeneous, investigating and quantifying the microstructure-tribofilm relationship of such materials has never been tried.

In this paper a detailed analysis of ZDDP tribofilms formed in non-conformal contacts on various bearing and gear steels under controlled rolling/sliding conditions is presented. The main focus is on establishing the impact of the microstructure of the underlying material on the morphology of the film. A great majority of the data used in this study was acquired with the recently developed AFM method [33] aimed at establishing correlations between the material and tribofilm.

## 2. Experimental

### *2.1. Tribochemical testing*

#### *2.1.1. Materials*

Four steel grades of distinctive chemical composition and microstructure were selected for testing to represent a wide spectrum of bearing and gear materials. These were: 100Cr6, 440C, M2 and 16MnCr5 steels. The chemical composition or these grades are listed in Table 1. All materials were provided by PCS Instruments, the test rig suppliers, as already heat treated, machined and finished specimens. **100Cr6** is a low alloy through hardened bearing steel. It is also the most popular bearing material [34]. After heat treatment typical for bearing applications (austenitisation at approximately 860 °C followed by quenching and tempering at about 160 °C) its microstructure consists of a tempered martensite matrix, 6-16 vol.% of retained austenite[1] [35, 36] and approximately 3-4 vol.% of residual carbides[2] [26]. The latter are normally present as spheroidal cementite ($M_3C$, where M stands for Fe or Cr) particles, about 0.3-1 μm in diameter [26, 27, 37, 38]. According to thermodynamic calculations performed by Barrow *et al.* [27] these contain more chromium than the surrounding matrix. Residual carbides are also harder than the tempered martensite matrix (Figure 1). **440C** is a through hardened stainless bearing steel. Due to a high chromium content it develops a layer of compact passive oxide on the surface, which provides protection against corrosion [39]. The microstructure of fully heat treated 440C steel comprises of tempered martensite, retained austenite and chromium rich residual carbides [40, 29]. Although no quantitative data on the volume fraction of residual carbides was reported by Hetzner *et al.* [29], a computational image analysis of the micrograph presented in Figure 4a of [29] yields approximately 15 vol.% of residual carbides. Two kinds of residual carbides may be distinguished in 440C steel: small ($< 3$ μm in diameter) spherical $M_{23}C_6$, and larger (up to few tens in μm in diameter) carbides of irregular shape, which are usually $M_7C_3$ surrounded by $M_{23}C_6$ [29]. Both types of carbides are richer in chromium [41, 42] and harder than the matrix (Figure 1). **M2** is a representative of high speed steels, although it is sometimes used for bearing applications [43]. In quenched and tempered condition the microstructure of M2 consists of tempered martensite, retained austenite, and residual carbides. Quenching from

[1] Parent austenite which did not transform to martensite during quenching.

[2] Carbides which are left undissolved during austenitisation prior to quenching.

the austenitisation temperature of 1220 °C results in approximately 10 vol.% of residual carbides [41]. About 90 vol.% of these are $M_6C$ carbides rich in heavy elements (molybdenum, tungsten) with the remaining 10 vol.% being vanadium-rich MC carbides [41]. Such carbides have significantly higher content of alloying elements than the matrix. Some of these carbides might be present together in a dual phase $M_6C - MC$ carbides, formed as a product of temperature-induced decomposition of metastable $M_2C$ carbide, which precipitate upon solidification [44]. Both types of carbides, especially MC, exhibit hardness significantly higher to that of the martensite (Figure 1). **16MnCr5** is different to the above listed materials, as it is a case carburising steel. As such, it is characterised by a low carbon content and, to achieve high surface hardness necessary for bearing and gear applications, prior to quenching and tempering the near-surface region (from ∼1 mm up to few mm) is usually diffusionally enriched in carbon at an elevated temperature (around 900°C) in a process called carburisation. The carbon enriched region is often called "case". As during bearing operation additives contained in the oil will react exclusively with the surface of the material, the case microstructure is critical from the viewpoint of tribochemistry, while the core microstructure remains less important. Limited information on 16MnCr5 steel microstructure is available in the literature, although reports on similar grades have been published. For 5120 steel 20 vol.% of retained austenite and no residual carbides have been reported in the case microstructure [45], and for 4118 steel, both retained austenite and residual carbides were observed in the case, but no quantitative results of their volume fraction were presented [46].

*2.1.2. Lubricants*

The lubricant employed in this study was custom-made with controlled formulation. A mixture of polyalphaolefin (PAO) with 10 vol.% of ester added to ensure the solubility of ZDDP was used as a base oil. Commercially available ZDDP was blended into the base oil to produce a mixture containing 0.08 wt.% P. The viscosity grade (ISO VG) of the base oil was 150 and its dynamic viscosity at the test temperature (80 °C) was 28.5 mPa·s.

*2.1.3. Test rig*

PCS mini traction machine (MTM) rig employing a ball-on-disc geometry (Figure 2) was used to produce tribofilms. The tribometer is connected to a computer controlling the rolling and sliding speeds (through independent

control of rotational speed of both samples), load and test temperature. The diameters of the disc and ball specimens were 46 mm and 19.05 mm respectively. Due to the geometry of sample arrangement, the track diameter on disc and ball are 42 mm and 17.35 mm respectively.

*2.1.4. Test procedure*

Prior to tribochemical tests all specimens were cleaned in an ultrasonic bath with toluene for 10 minutes and with isopropanol for another 10 minutes. Subsequently, specimens were mounted on the tribometer and an amount of oil sufficient to just cover the surface of the disc was poured into the test chamber. Lubricant was then allowed to heat up to the desired temperature and the test was commenced. The test conditions are specified in Table 2. The entrainment speed, $v_{entr}$, and slide-roll ratio, SRR, listed in Table 2, are calculated according to the following equations:

$$v_{entr} = \frac{v_b + v_d}{2} \tag{1}$$

$$\mathrm{SRR} = 2\frac{|v_b - v_d|}{v_b + v_d} \tag{2}$$

where $v_b$ and $v_b$ are ball and disc surface velocities, respectively, as indicated in Figure 2. The contact zone radius, $a$, and the maximum contact pressure, $p_{max}$, in Table 2 were calculated according to Hertzian contact theory [52, 53]. At the start of the testing programme a Stribeck curve was obtained at the specified test load and slide-roll ratio. Subsequently, the test speed of 35 mm/s was chosen because it is low enough to ensure mixed lubrication conditions (i.e. some metal-to-metal contact) in all tests favouring formation of ZDDP boundary films, while allowing for relatively fast accumulation of rubbing distance.

Tribochemical tests were run using the four different steel grades but the same lubricant. Fresh samples and fresh oil were used in each run. In all tests both specimens (ball and disc) were made from the same material. Table 3 lists hardness, roughness and resultant dimensionless lubricant film thickness, $\lambda$, which was calculated from following formula:

$$\lambda = \frac{h_0}{\sqrt{R_{rms,b}^2 + R_{rms,d}^2}} \tag{3}$$

where $h_0$ is the minimum elastohydrodynamic lubricant film thickness and $R_{rms,d}$ and $R_{rms,b}$ denote disc and ball specimen root mean square roughness. The minimum elastohydrodynamic lubricant film thickness was calculated according to Hamrock-Dowson equation [54]. In all cases $h_0$ was equal to 7.3 nm. This value was obtained by assuming that Young's moduli and Poisson's ratios of all tested steel grades are equal to 210 GPa and 0.3 respectively.

### *2.2. Tribofilm and microstructure analysis*

#### *2.2.1. Sectioning*

After completing a tribochemical test and removing the samples from the rig, the discs were sectioned into specimens of a size allowing analysis with an optical microscope, stylus profilometer and AFM. Subsequently, specimens were ultrasonically cleaned in toluene for 10 minutes and in isopropanol for another 10 minutes to remove any residual oil[3]. Only disc specimens were analysed due to lack of curvature of the film-containing surface, facilitating analysis with the employed techniques. This is in contrast to the standard technique of measuring ZDDP boundary films, which uses spacer layer imaging method (SLIM), built directly into the MTM, to measure out-of-contact ZDDP films on the MTM ball specimen [55].

#### *2.2.2. Optical microscopy*

Optical microscope was employed to analyse the microstructure of the investigated steel grades, to confirm the formation of the tribofilm in the tribochemical tests, to monitor the experimental sequence used in stylus profilometry and AFM methods and to provide supplementary data for these techniques. All optical micrographs were taken with a Leica DM 2500M microscope.

#### *2.2.3. Stylus profilometry*

Stylus profilometry was used to measure the average tribofilm thickness and wear of the substrate material. This was performed by acquiring surface

[3] The influence of both solvents on the tribofilm was investigated by ultrasonically cleaning dummy samples in toluene or in isopropanol for 5 minutes, for an additional 10 minutes (totalling to 15 minutes) and for an additional 30 minutes (totalling to 45 minutes). Samples were observed under the optical microscope at each step. No difference between the appearance of the tribofilm or any form tribofilm dissolution was noted. Figure S1 presents optical micrographs taken at each step of this experiment.

profiles across the racetrack in two conditions (1) before removal of the tribofilm (referred to as "preEDTA" profiles); (2) after removing the tribofilm with 0.2 mol/litre ethylenediaminetetraacetic acid (EDTA) disodium salt in distilled water solution as applied by Topolovec-Miklozic *et al.* [13] (referred to as "postEDTA" profiles). A pattern of microindents was arranged on the sample prior to profilometry experiments to ensure that the same lines are scanned at each step. Profiles were acquired at 5 different locations (approximately 10 profiles per location) at each step. Subsequently, software developed in-house was used to correct the offset between profiles (microindents were used as reference points) and calculate the tribofilm thickness by subtracting postEDTA profiles from preEDTA profiles. Wear volume was calculated by numerically integrating the postEDTA profiles and multiplying by the track length. Erratic profiles, e.g. ones with abrupt steps due to presence of debris on the specimen, were excluded from the analyses. All profiles were acquired with Veeco Dektak 6M apparatus. A detailed description of the experimental procedure and data analysis process can be found in [56].

*2.2.4. Atomic force microscopy (AFM)*

A recently developed AFM method, designed specially for that purpose, was used to analyse the dependence between morphology of the tribofilm and the microstructure of the underlying material. A detailed description of the method can be found elsewhere [33, 56]. A general concept of the method is similar to the stylus profilometry procedure described above, although employing AFM greatly extends the capabilities of this approach by providing high resolution three-dimensional data and allowing observation of the microstructure of the substrate material by performing an additional scan after removing the tribofilm and etching the specimen to reveal the microstructure. Three micrographs for each region are obtained. These are:

1. "preEDTA" micrograph acquired after cleaning the sample, but before removing the tribofilm, showing the morphology of the film
2. "postEDTA" micrograph acquired after removing the tribofilm with EDTA, showing the topography of the underlying material
3. "as-etched" micrograph acquired after etching the steel with appropriate etchant, showing the microstructure of the steel

Because EDTA treatment allows to entirely remove the ZDDP tribofilm without any effect on the substrate material, it enables generating tribofilm thickness maps by subtracting the postEDTA micrograph from the preEDTA

micrograph. This may subsequently be compared with as-etched AFM micrograph showing the microstructure of the underlying material to determine the impact of given microstructural features. The etchants used in this study (2% nital for 100Cr6, M2 and 16MnCr5 steels and glyceregia for 440C steel) usually dissolve the tempered martensite matrix while leaving residual carbides intact. Due to the character of AFM data (each point has its x, y and z coordinate), micrographs may be used in a quantitative way for correlating the local tribofilm thickness with the microstructure of the material.
To achieve an optimal compromise between the investigated surface area, the lateral resolution and the scan time, the size of AFM micrographs used in this study was set to 50 μm by 50 μm. Due to necessity of imaging microindents which act as reference points for the employed AFM method, the usable surface area, not affected by microindents, is even smaller, approximately 30 μm by 30 μm. Because this is a few times smaller than the width of the rubbing track on the MTM disc, it may cause a bias resulting from positioning the area investigated with the AFM with respect to the rubbing track width. In order to exclude such selectivity, a pattern of microindents extending across the whole tribofilm width was arranged on the surface, as shown in Figure 3. Each of the marked squares (these are referred to as "zones") was investigated and analysed independently with respect to average tribofilm thickness on the matrix and residual carbides (in a given zone) and other parameters, allowing plotting these parameters as a function of the distance across the track to provide a more general insight into the tribofilm-microstructure correlation for each specimen. Subsequently, separate AFM micrographs and profiles extracted from the AFM data of each steel grade and were inspected to provide better understanding on the impact of the microstructure on the tribofilm.
All AFM micrographs were taken with a Bruker Nanoscope Multimode microscope operating in the intermittent contact mode.

## 3. Results

PreEDTA and postEDTA optical micrographs of tested MTM discs are presented in Figure 4. PreEDTA micrographs (upper part of the figure) clearly show that the tribofilm has developed in all cases. Tribofilm thickness measured by stylus profilometry is also indicated in the figure, showing that relatively thick (over 50 nm) tribofilm has formed in each case. For each sample the central 250 μm of the tribofilm, as exemplified with red bars in

Figure 4, was used to measure the average tribofilm thickness. Micrographs taken after tribofilm removal (bottom part of Figure 4) shows that ZDDP tribofilm can be completely dissolved by EDTA treatment. No statistically significant wear was measured by stylus profilometry on any of the samples.

In Figure 5 high magnification optical micrographs showing the tribofilm and microstructure of the underlying material (after tribofilm removal and etching) are presented. The same region (central 1/3 of the tribofilm) is shown in both micrographs for a given grade. Some areas, that in the preEDTA micrographs appear to have lower tribofilm thickness or no tribofilm at all, correspond to microstructural features visible in as-etched micrographs. For clarity, the most apparent areas exhibiting such correspondence are marked with black circles or ellipses, located it the same positions in both micrographs. In most cases such areas are associated with residual carbides. This effect is most profound in high alloyed steels (440C and M2) where large residual carbides are present; and is less marked in 100Cr6 steel, in which residual carbides are smaller and occupy lower volume fraction. In 16MnCr5 steel one of the tribofilm-free spots seems to be related with a block of retained austenite lying underneath, although this might be a random occurrence.

The tribofilm-microstructure correlation can be readily observed in the presented optical micrographs, but these do not allow quantifying this relationship and relating it to the topography of the underlying substrate. For that reason the specimens were studied in detail with the AFM method.

### *3.1. Atomic force microscopy (AFM)*

#### *3.1.1. Tribofilm thickness profiles*

Graphs showing the tribofilm thickness on martensitic matrix and residual carbides across the tribofilm are presented in Figure 6. The distance in Figure 6 is measured from the outer boundary of the rubbing track towards the centre of the MTM disc. It is apparent in Figure 6 that tribofilm tends to be thinner on residual carbides than on the matrix in most of the cases. The overall tribofilm thickness is not plotted, as in each case this was very close to that of the martensitic matrix owing to the fact that the matrix occupies 80% or more of the surface area. Due to that, as a result of small errors in correcting for the relative displacement between the preEDTA, postEDTA and as-etched AFM micrographs, the average tribofilm thickness on residual carbides might be overestimated, and in reality the film thickness on carbides might be even lower than shown in the figure. The film thickness

profile exhibits similar overall characteristics in all four cases, with the film thickness increasing gradually for the first ∼1/3 of the rubbing track width, then stabilising for another ∼1/3 of the width and subsequently decreasing. Film thickness peaks in 440C and 16MnCr5 profiles are thought to be related to an occurrence of large tribofilm patches in the corresponding zones. The reason for the local minima of film thickness observed in the middle of the track, most evident in the case of 100Cr6 and M2 steels are not clear, but these may be related to film non-uniformity or caused by the slip distribution within the contact zone and/or an increased level of wear in these regions, resulting from the higher local contact pressures.

*3.1.2. Impact of carbide protrusion*

Figure 6 shows that the tribofilm thickness on the martensitic matrix is usually higher than on residual carbides. It is known that due to their higher hardness residual carbides tend to protrude from the surface, especially in tribological conditions involving some wear. Taking the carbide protrusion into account, there are two boundary cases in which lower tribofilm thickness on carbides could be achieved:

1. Residual carbides do not protrude from the surface at all, but the tribofilm grows dissimilarly on residual carbides and on the matrix (Figure 7a).
2. Residual carbides stick out from the surface, but the tribofilm grows to a similar overall level both on residual carbides and on the matrix. Hence, the tribofilm fills the valleys between residual carbides (Figure 7b).

In reality both scenarios may be expected to operate simultaneously. To quantify the extent of each of these effects as-etched AFM data were used to calculate the average carbide protrusion in each zone. This was then compared with the tribofilm thickness on carbides and the matrix, as shown in Figure 8. Figure 9 explains the way in which the data are plotted.

*3.1.3. 100Cr6 steel*

For 100Cr6 the influence of carbides on ZDDP film thickness is inconclusive. As shown in Figure 6a, in most zones, particularly those lying in the middle of the rubbing track, the average film thickness on residual carbides is lower than on the martensitic matrix. Figures 8 and 10 indicate that the average film thickness does not correlate with the carbide protrusion.

On the other hand, although the correspondence between some residual carbides and the tribofilm-free areas is observed (as exemplified in Figure 5 and AFM micrographs and tribofilm thickness map shown in Figure S2) only a small fraction of residual carbides are associated with "holes" in the film and many carbides are entirely covered by relatively thick tribofilm, often of the same thickness as the martensitic matrix.

*3.1.4. 440C steel*

In the case of 440C steel, in most zones the film thickness on carbides and matrix is the same (Figure 6b), despite pronounced protrusion of the carbides (Figure 8b). The exception was the fourth zone, where the film is significantly thinner on carbides. This is most likely associated with the presence of a large residual carbide approximately in the middle of that zone. Figure 11a-d show AFM micrographs and a film thickness map of that region. The profiles extracted from the AFM data, presented in Figure 11e, visualise the correspondence between carbides and thinner film. Nevertheless, the marked carbide is not left entirely film-free and a thick film covers the edge of it together with the adjacent matrix. This observation may indicate that the film is mechanically "deposited" against the protruding carbide during rolling/sliding motion.

An opposite effect was observed in zones lying at the boundaries of the rubbing track, where the tribofilm has preferentially formed on large residual carbides, despite their pronounced protrusion from the matrix. This is exemplified in Figure 12a, which presents profiles extracted from the AFM micrographs of a single zone located at the edge of the track. AFM micrographs associated with Figure 12a are presented in Figure S3. Black arrows in Figure 12a indicate positions of residual carbides on which the film has preferentially formed. In addition, on several dual-phase large residual carbides, a preferential tribofilm formation on $M_7C_3$ with respect to $M_{23}C_6$ was observed as exemplified in Figure 13. This might be related to the hardness difference between these two carbide types (Figure 1) that would most likely result in more pronounced protrusion of $M_7C_3$, their chemical composition ($M_7C_3$ are richer in Cr than $M_{23}C_6$), or some other effects.

Except for the zone lying at the edge of the rubbing track (shown in Figure S3) the large residual carbide was present in only one of the investigated zones (zone 4 shown in Figure 11). For that reason a further confirmation of the correspondence between large carbides and film-free areas was required. As it was already known that large regions without any tribofilm are likely

to be related to carbides an additional sample was prepared. Instead of arranging an usual pattern of microindents extending across the whole track, three square zones were marked at locations that appeared to be related with residual carbides, as shown in Figure S4. Subsequently, these additional zones were investigated with the proposed AFM procedure. In all three cases these have proven to contain a large carbide characterised by thinner tribofilm as exemplified in Figure 12b. AFM micrographs used to extract data shown in Figure 12b are presented in Figure S5. As evident from Figure 12, these carbides protrude from the surface by approximately 70 nm.

*3.1.5. M2 steel*

The tribofilm formed on M2 steel is thinner on residual carbides than on the martensitic matrix across the whole rubbing track width. This effect is not solely caused by carbide stick-out, as Figure 8c shows that the differences in tribofilm thickness between matrix and carbides are larger than the carbide protrusion. The relationship between microstructure and the tribofilm is also clearly visible in the AFM micrographs and film thickness map (Figure 14a-d), especially for the large carbide cluster shown in the lower left corner of the micrographs. The SEM micrograph in Figure 14e and associated energy-dispersive X-ray spectroscopy (EDX) maps in Figure 14f-i show that the great majority of residual carbides in this zone are W and Mo rich $M_6C$, with the rest being V-rich MC, and that the carbide cluster consists mostly of $M_6C$ with some MC. The proportion of $M_6C$ to MC was very similar also in other zones used to generate Figure 6c and Figure 8c, and similar clusters were commonly observed. Profiles generated from the AFM data cutting through the $M_6C + MC$ cluster (Figure 14f) reveal that it protrudes from the surface by $\sim$50 nm and is covered by thinner tribofilm than the surrounding matrix. Similar behaviour was noted for $M_6C$ carbides and $M_6C + MC$ clusters in other zones, as exemplified in the optical micrographs presented in Figure 5.

No large MC carbides were observed in any of the zones initially investigated with the AFM on the M2 specimen, although such carbides were observed in the metallographic samples from that steel. For that reason, similarly to 440C case, an additional specimen aimed at studying the impact of large primary MC carbides on the tribofilm was prepared. Two zones containing tribofilm-free areas were marked, as shown in Figure S6a. These were subsequently investigated with the AFM method using the proposed procedure. After removing the tribofilm, both zones proved to be related to a large

vanadium-rich MC carbides[4] (Figure S6b). Profiles from the AFM data (Figure 12c) unveil that these carbides are covered by almost no tribofilm. They protrude from the surface by ∼100 nm, fact which may be responsible for the lack of the tribofilm, as these would be much more exposed to wear than the surrounding matrix, given that the minimum predicted elastohydrodynamic lubricant film thickness was 7.3 nm and the contact was operating in the mixed lubrication regime. AFM micrographs and film thickness map associated with Figure 12c are presented in Figure S8a-d. Pronounced protrusion of MC carbide is well visible in the postEDTA micrograph shown in Figure S8b enabling easy identification even without any etching and lack of the tribofilm on the carbide is confirmed by the film thickness map presented in Figure S8d.

*3.1.6. 16MnCr5 steel*

Despite the lack of residual carbides in the 16MnCr5 steel, the tribofilm formed by ZDDP on this grade also has patch-like morphology as shown in Figure 5. Profiles extracted from the AFM data (Figure 12d) show that the pattern of film islands is very regular with a consistent spacing between the pads. Figure S9a-c show the AFM data that were used to generate the profiles shown in Figure 12d. The regularity of the film patches probably stems from the absence of residual carbides, however, some larger film-free areas are also present. The tribofilm morphology and lack of residual carbides in the 16MnCr5 sample is also well visible in the AFM micrographs and associated tribofilm thickness map presented in Figure S9.

## 4. Discussion

The results presented here show that the morphology of ZDDP tribofilms is affected by, amongst other factors, to the microstructure of the underlying steel, with residual carbides being the main microstructural feature observed to affect the local tribofilm thickness. The tribofilm on residual carbides is

[4] The differentiation between $M_6C$ and MC by colour under the optical microscope is mostly based on the optical microscope and SEM/EDX observation of the same region of the specimen performed in-house. During such observations it was noted that under the optical microscope V-rich MC carbides exhibit red/pink colouring, whereas W- and Mo-rich $M_6C$ appear white. Figure S7 presents optical and SEM micrographs and associated EDX spectra of $M_6C$ and MC carbides.

usually non-existent or significantly thinner with respect to the surrounding tempered martensite matrix. Even when the carbide protrusion is compensated for, the tribofilm is still observed to be significantly thinner on residual carbides than on martensitic matrix in most cases. This means that the film thickness differences between carbides and matrix are not a direct result of developing a smooth tribofilm on a initially rough substrate containing surface peaks caused by the presence of residual carbides (as illustrated in Figure 7b). Although residual carbides were shown to have an important impact on the morphology of the film, results obtained with 16MnCr5 steel prove that even when the carbides are absent ZDDP still forms a patch-like tribofilm.

With the exception of large protruding residual carbides lying at the edge of the tribofilm formed on 440C steel, the correlation between the location of the film islands and asperities on the substrate material suggested by [22, 23, 7] was not observed in any of the investigated samples. Nonetheless, despite the fact that no statistically significant wear was measured on any of the tested specimens, it is possible that asperities, initially present on the sample, that were tribofilm nucleation sites were removed during tribochemical tests due micro-scale wear or digested by ZDDP as a result of its reactions with the steel. Moreover, it should be noted that this study was conducted with very smooth disc specimens (disc Ra<15 nm in all cases), therefore, it is possible that in the case of higher surface roughness asperities would impact the film in a more significant way.

The tribofilm develops only on the track, with the film width (as shown in the Figure 4) corresponding well with the size of the contact zone calculated using Hertzian contact theory (enlisted in Table 2), suggesting that the mechanical interaction between counterparts in the contact zone is necessary for the tribofilm development under the employed test conditions.

According to Aktary *et al.*[7] ZDDP film develops via nucleation and growth mechanism, with asperities or "active sites at the steel surface" being the nucleation sites. Based on the experimental data summarised above, extending the concept of Aktary *et al.* as follows is suggested. Mechanical contact is necessary to form ZDDP tribofilm. This is manifested both on macro- (no tribofilm develops outside the track) and micro-scale (tribofilm forms patches most likely by nucleating on asperities). Among the regions exposed to mechanical interaction, certain regions in the microstructure of the substrate material are more effective in developing the tribofilm as a result of effects of chemical nature, such as different affinity of ZDDP to

given elements or dissimilarities in ZDDP adsorption efficiency on various microstructure components. Moreover, the tribofilm wear behaviour of the microstructural features is most likely also dissimilar, e.g. as a result of film adhesion variations, what may introduce additional differences in the observed final tribofilm thickness among the microstrucure constituents.
In the light of such hypothesis many of the observed tribofilm-microstructure interactions may be rationalised. The tribofilm patchiness on 16MnCr5 specimen, which did not contain any residual carbides, presumably result from the surface roughness that is either to fine to be resolved with employed technique or was removed by wear or digested due to ZDDP reactions on course of the tribochmical test. It is also possible that certain microstructural features that were not considered in this study, such as grain boundaries or other crystallographic defects, are preferred sites for tribofilm nucleation, contributing to the resultant film roughness. Therefore under the employed testing conditions even the microstructure consisting solely of tempered martensite matrix exhibit some inherent roughness. More complex behaviours are observed once residual carbides are present in the microstructure. In case of 100Cr6, 440C and M2 steels the martensitic matrix shows similar intrinsic tribofilm patchiness, but the film is additionally disturbed by the presence of residual carbides, which in 100Cr6 and M2 steels seem to be unfavourable sites for tribofilm development regardless of their protrusion from the surface.
The most complex behaviour is observed in the case of 440C, where the tribofilm is preferentially formed on large protruding carbides, if these are located in the outer parts of the track, but same type of carbide is often bare when present in the middle of the track. This can be rationalised by interpreting the measured film thickness as a result of a balance between the film formation by chemical reaction and its removal by wear. According to that, it can be hypothesised that due to carbide protrusion or due to differences in chemical composition between matrix and carbides ZDDP reaction kinetics with the latter is higher, resulting in initially thicker tribofilm. Carbides with preferentially formed tribofilm act as asperities, and therefore are more exposed to wear, especially in the middle of the track where lubricant elastohydrodynamic film is thinner and contact pressure is higher. As a result, the tribofilm is removed from carbides, likely via a decohesion mechanism, as large areas of carbides are often observed to be bare. Once tribofilm is removed from the carbide, it can not be rebuilt because the carbide no longer exhibits localised mechanical contact, as the load is carried by the tribofilm that has developed on the surrounding martensitic matrix in the meantime

(although likely with slower kinetics). Such theory would also explain why in 440C mainly large carbides are observed to correlate with tribofilm-free areas, while smaller carbides are often fully covered by the tribofilm. In such a case, it is possible that the tribofilm patch that has developed over the matrix surrounding smaller carbides and the carbides themselves is able to provide sufficient adhesion to prevent tribofilm decohesion from the carbide. Moreover, lateral growth of the tribofilm nucleated on the martensitic matrix, but extending over carbides likely contributes to that effect. Lateral film growth from the matrix would also explain why many small carbides (e.g. $M_6C$ in M2 steel and $M_3C$ in 100Cr6 steel), despite the fact that these probably are unfavourable sites for the tribofilm development, are fully covered by the tribofilm and only a fraction of these small carbides are observed to correlate with the film-free regions.

## 5. Summary and conclusions

Tribofilms derived from ZDDP on four different hard steel grades used in tribological applications under controlled conditions were investigated by employing a recently developed AFM technique to establish the correlation between the microstructure of the substrate material and the morphology of the film. The results can be summarised as follows:

1. Local ZDDP tribofilm thickness is affected by the microstructure of the underlying steel.
2. In general the tribofilm was observed to be significantly thinner on residual carbides than on the martensitic matrix, but there are important exceptions to this.
3. ZDDP forms patch-like tribofilm even when residual carbides are absent.
4. The differences of tribofilm thickness on the matrix and on residual carbides are usually larger than carbide protrusion.
5. The type and size of carbide was observed to be important in terms of its impact on ZDDP film. Large carbides, especially MC carbides and $M_6C$ + MC clusters in M2 steel and $M_7C_3 + M_{23}C_6$ dual phase carbides in 440C steel are more likely to correspond to tribofilm-free areas than smaller carbides.
6. Large $M_7C_3 + M_{23}C_6$ residual carbides in 440C steel exhibit preferential or unfavoured tribofilm build-up with respect to the martensitic matrix

depending on their location across the rubbing track. Carbides located approximately in the centre of the tribofilm are often tribofilm-free, whereas those lying at the boundaries of the tribofilm usually show preferential tribofilm formation with respect to adjacent matrix.

**Acknowledgements**

The authors are grateful to Prof. Mark Blamire for the provision of laboratory facilities, and to SKF and Afton Chemical for financial support. The consultation and help provided by Dr Nadia Stelmashenko, Dr Isaac Toda-Caraballo, Dr Marc Ingram and Dr Erik Vegter is also greatly acknowledged.

**References**

[1] H. A. Spikes, "The history and mechanisms of ZDDP," *Tribology Letters*, vol. 17, no. 3, pp. 469–489, 2004.

[2] A. M. Barnes, K. D. Bartle, and V. R. Thibon, "A review of zinc dialkyldithiophosphates (ZDDPs): characterisation and role in the lubricating oil," *Tribology International*, vol. 34, no. 6, pp. 389–395, 2001.

[3] A. J. Gellman and N. D. Spencer, "Surface chemistry in tribology," *Proceedings of the Institution of Mechanical Engineers, Part J: Journal of Engineering Tribology*, vol. 216, no. 6, pp. 443–461, 2002.

[4] S. Equey, S. Roos, U. Mueller, R. Hauert, N. D. Spencer, and R. Crockett, "Reactions of zinc-free anti-wear additives in DLC/DLC and steel/steel contacts," *Tribology International*, vol. 41, no. 11, pp. 1090–1096, 2008.

[5] L. J. Taylor, H. A. Spikes, and H. Camenzind, "Film-forming properties of zinc-based and ashless antiwear additives," *SAE Technical Paper 2000-01-2030*, 2000.

[6] J. F. Graham, C. McCague, and P. R. Norton, "Topography and nanomechanical properties of tribochemical films derived from zinc dialkyl and diaryl dithiophosphates," *Tribology Letters*, vol. 6, no. 3-4, pp. 149–157, 1999.

[7] M. Aktary, M. T. McDermott, and G. A. McAlpine, "Morphology and nanomechanical properties of ZDDP antiwear films as a function of tribological contact time," *Tribology Letters*, vol. 12, no. 3, pp. 155–162, 2002.

[8] H. Fujita and H. A. Spikes, "The formation of zinc dithiophosphate antiwear films," *Proceedings of the Institution of Mechanical Engineers, Part J: Journal of Engineering Tribology*, vol. 218, no. 4, pp. 265–278, 2004.

[9] M. N. Najman, M. Kasrai, and G. M. Bancroft, "Chemistry of antiwear films from ashless thiophosphate oil additives," *Tribology Letters*, vol. 17, no. 2, pp. 217–229, 2004.

[10] M. N. Najman, M. Kasrai, G. M. Bancroft, B. H. Frazer, and G. De Stasio, "The correlation of microchemical properties to antiwear (AW) performance in ashless thiophosphate oil additives," *Tribology Letters*, vol. 17, no. 4, pp. 811–822, 2004.

[11] A. Tomala, A. Naveira-Suarez, I. C. Gebeshuber, and R. Pasaribu, "Effect of base oil polarity on micro and nanofriction behaviour of base oil+ZDDP solutions," *Tribology-Materials, Surfaces & Interfaces*, vol. 3, no. 4, pp. 182–188, 2009.

[12] A. Naveira-Suarez, *The behaviour of antiwear additives in lubricated rolling-sliding contacts*. PhD thesis, Luleå Tekniska Universitet, 2011.

[13] K. Topolovec-Miklozic, T. R. Forbus, and H. A. Spikes, "Film thickness and roughness of ZDDP antiwear films," *Tribology Letters*, vol. 26, no. 2, pp. 161–171, 2007.

[14] K. Topolovec-Miklozic and H. A. Spikes, "Application of atomic force microscopy to the study of lubricant additive films," *Journal of Tribology*, vol. 127, no. 2, pp. 405–415, 2005.

[15] Y.-R. Li, G. Pereira, M. Kasrai, and P. R. Norton, "The effect of steel hardness on the performance of ZDDP antiwear films: a multi-technique approach," *Tribology Letters*, vol. 29, no. 3, pp. 201–211, 2008.

[16] L. J. Taylor and H. A. Spikes, "Friction-enhancing properties of ZDDP antiwear additive: part I — friction and morphology of ZDDP reaction films," *Tribology Transactions*, vol. 46, no. 3, pp. 303–309, 2003.

[17] L. J. Taylor, A. Dratva, and H. A. Spikes, "Friction and wear behavior of zinc dialkyldithiophosphate additive," *Tribology Transactions*, vol. 43, no. 3, pp. 469–479, 2000.

[18] O. Warren, J. Graham, P. Norton, J. Houston, and T. Michalske, "Nanomechanical properties of films derived from zinc dialkyldithiophosphate," *Tribology Letters*, vol. 4, no. 2, pp. 189–198, 1998.

[19] Z. Yin, M. Kasrai, M. Fuller, G. M. Bancroft, K. Fyfe, and K. H. Tan, "Application of soft X-ray absorption spectroscopy in chemical characterization of antiwear films generated by ZDDP Part I: the effects of physical parameters," *Wear*, vol. 202, no. 2, pp. 172–191, 1997.

[20] R. Kapadia, R. Glyde, and Y. Wu, "In situ observation of phosphorous and non-phosphorous antiwear films using a mini traction machine with spacer layer image mapping," *Tribology International*, vol. 40, no. 10, pp. 1667–1679, 2007.

[21] L. J. Taylor and H. A. Spikes, "Friction-enhancing properties of ZDDP antiwear additive: part II — influence of ZDDP reaction films on EHD lubrication," *Tribology Transactions*, vol. 46, no. 3, pp. 310–314, 2003.

[22] N. J. Mosey, T. K. Woo, M. Kasrai, P. R. Norton, G. M. Bancroft, and M. H. Müser, "Interpretation of experiments on ZDDP anti-wear films through pressure-induced cross-linking," *Tribology Letters*, vol. 24, no. 2, pp. 105–114, 2006.

[23] G. Canning, M. S. Fuller, G. Bancroft, M. Kasrai, J. Cutler, G. De Stasio, and B. Gilbert, "Spectromicroscopy of tribological films from engine oil additives. Part I. Films from ZDDP's," *Tribology Letters*, vol. 6, no. 3-4, pp. 159–169, 1999.

[24] K. Ito, J. M. Martin, C. Minfray, and K. Kato, "Formation mechanism of a low friction ZDDP tribofilm on iron oxide," *Tribology Transactions*, vol. 50, no. 2, pp. 211–216, 2007.

[25] M. L. S. Fuller, M. Kasrai, G. M. Bancroft, K. Fyfe, and K. H. Tan, "Solution decomposition of zinc dialkyl dithiophosphate and its effect on antiwear and thermal film formation studied by X-ray absorption spectroscopy," *Tribology International*, vol. 31, no. 10, pp. 627–644, 1998.

[26] H. K. D. H. Bhadeshia, "Steels for bearings," *Progress in Materials Science*, vol. 57, no. 2, pp. 268–435., 2012.

[27] A. T. W. Barrow, J.-H. Kang, and P. E. J. Rivera-Díaz-del Castillo, "The $\epsilon \rightarrow \eta \rightarrow \theta$ transition in 100Cr6 and its effect on mechanical properties," *Acta Materialia*, vol. 60, no. 6, pp. 2805–2815, 2012.

[28] J. E. Bridge, G. N. Maniar, and T. V. Philip, "Carbides in M50 high-speed steel," *Metallurgical Transactions*, vol. 2, pp. 2209–2214, 1971.

[29] D. W. Hetzner and W. Van Geertruyden, "Crystallography and metallography of carbides in high alloy steels," *Materials Characterization*, vol. 59, no. 7, pp. 825–841, 2008.

[30] R. D. Evans, G. L. Doll, C. Hager, and J. Y. Howe, "Influence of steel type on the propensity for tribochemical wear in boundary lubrication with a wind turbine gear oil," *Tribology Letters*, vol. 38, no. 1, pp. 25–32, 2010.

[31] M. A. Nicholls, P. R. Norton, G. M. Bancroft, M. Kasrai, G. D. Stasio, and L. M. Wiese, "Spatially resolved nanoscale chemical and mechanical characterization of ZDDP antiwear films on aluminum–silicon alloys under cylinder/bore wear conditions," *Tribology Letters*, vol. 18, no. 3, pp. 261–278, 2005.

[32] X. Xia, A. Morina, A. Neville, M. Priest, R. Roshan, C. Warrens, and M. Payne, "Tribological performance of an Al–Si alloy lubricated in the boundary regime with zinc dialkyldithiophosphate and molybdenum dithiocarbamate additives," *Proceedings of the Institution of Mechanical Engineers, Part J: Journal of Engineering Tribology*, vol. 222, no. 3, pp. 305–314, 2008.

[33] J. J. Rydel, R. Vegter, and P. Rivera-Díaz-del Castillo, "Tribochemistry of bearing steels: A new AFM method to study the material–tribofilm correlation," *Tribology International*, vol. 98, pp. 74–81, 2016.

[34] E. V. Zaretsky, "Rolling bearing steels—a technical and historical perspective," *Materials Science and Technology*, vol. 28, no. 1, pp. 58–69, 2012.

[35] J. Beswick, "Fracture and fatigue crack propagation properties of hardened 52100 steel," *Metallurgical Transactions A*, vol. 20, no. 10, pp. 1961–1973, 1989.

[36] R. Banerjee, "X-ray determination of retained austenite," *Journal of Heat Treating*, vol. 2, no. 2, pp. 147–150, 1981.

[37] C. A. Stickels, "Carbide refining heat treatments for 52100 bearing steel," *Metallurgical Transactions*, vol. 5, no. 4, pp. 865–874, 1974.

[38] P. Daguier, O. Roesch, and W. Trojahn, "New development in through hardened bearing steel grades for use in contaminated lubrication," *ASTM Special Technical Publication 1465*, pp. 131–139, 2007.

[39] *ASM Handbook: Vol. 1: Properties and selection: irons, steels, and high performance alloys*. ASM International, 1990.

[40] J. R. Yang, T. H. Yu, and C. H. Wang, "Martensitic transformations in AISI 440C stainless steel," *Materials Science and Engineering: A*, vol. 438, pp. 276–280, 2006.

[41] G. A. Roberts, R. Kennedy, and G. Krauss, *Tool steels*. ASM international, 1998.

[42] S. Salleh, M. Z. Omar, J. Syarif, M. Ghazali, S. Abdullah, and Z. Sajuri, "Investigation of microstructures and properties of 440C martensitic stainless steel," *International Journal of Mechanical and Materials Engineering*, vol. 4, no. 2, pp. 123–126, 2009.

[43] P. K. Pearson, "The history and future of aircraft turbine engine bearing steels," *ASTM Special Technical Publication 1327*, pp. 335–353, 1998.

[44] X. F. Zhou, F. Fang, J. Q. Jiang, W. L. Zhu, and H. X. Xu, "Study on decomposition behaviour of $M_2C$ eutectic carbide in high speed steel," *Materials Science and Technology*, vol. 28, no. 12, pp. 1499–1504, 2012.

[45] K. Burkart, H. Bomas, and H.-W. Zoch, "Fatigue of notched case-hardened specimens of steel SAE 5120 in the VHCF regime and application of the weakest-link concept," *International Journal of Fatigue*, vol. 33, no. 1, pp. 59–68, 2011.

[46] C. F. Yang, L. H. Chiu, and J. K. Wu, "Effects of carburization and hydrogenation on the impact toughness of AISI 4118 steel," *Surface and Coatings Technology*, vol. 73, no. 1, pp. 18–22, 1995.

[47] A. Kagawa, T. Okamoto, K. Saito, and M. Ohta, "Hot hardness of $(Fe, Cr)_3C$ and $(Fe, Cr)_7C_3$ carbides," *Journal of Materials Science*, vol. 19, no. 8, pp. 2546–2554, 1984.

[48] H. Brandis, E. Haberling, and H. H. Weigand, "Metallurgical aspects of carbides in high-speed steels," *Processing and Properties of High-Speed Tool Steels*, pp. 1–18, 1980.

[49] R. Wilson, *Metallurgy and heat treatment of tool steels*. McGraw-Hill Companies, 1975.

[50] L. Tarasov, "The microhardness of carbides in tool steels," *Metal Progress*, vol. 54, p. 846, 1948.

[51] P. Leckie-Ewing, "A study of the microhardness of the major carbides in some high speed steels," *Transactions of the American Society for Metals*, vol. 44, pp. 348–366, 1952.

[52] K. L. Johnson, *Contact mechanics*. Cambridge University Press, 1987.

[53] G. Stachowiak and A. W. Batchelor, *Engineering tribology*. Butterworth-Heinemann, 2013.

[54] B. J. Hamrock and D. Dowson, "Isothermal elastohydrodynamic lubrication of point contacts: part III-fully flooded results," *Journal of Lubrication Technology*, vol. 99, no. 2, pp. 264–275, 1977.

[55] P. M. Cann, H. A. Spikes, and J. Hutchinson, "The development of a spacer layer imaging method (SLIM) for mapping elastohydrodynamic contacts," *Tribology transactions*, vol. 39, no. 4, pp. 915–921, 1996.

[56] J. Jelita Rydel, *Tribochemistry of bearing steels*. PhD thesis, University of Cambridge, 2016.

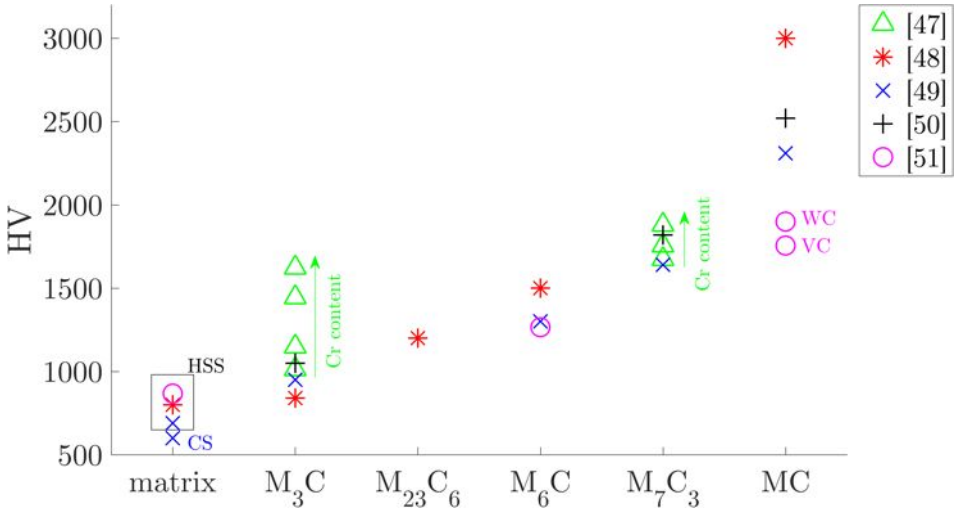


Figure 1: Hardness of carbides and matrix in martensitic steels. Annotations on differences in chemical composition among a single carbide type (or for the martensitic matrix) are marked where relevant. HSS and CS denote high speed steel and carbon steel respectively. VC an WC denote vanadium and tungsten carbide respectively.

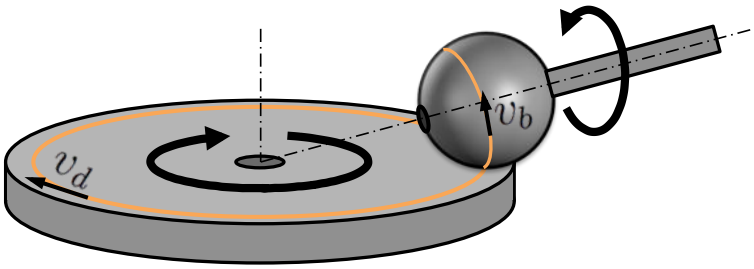


Figure 2: Schematic representation of the sample arrangement in the MTM rig (side view). $v_b$ and $v_d$ denote disc and ball surface velocities respectively.

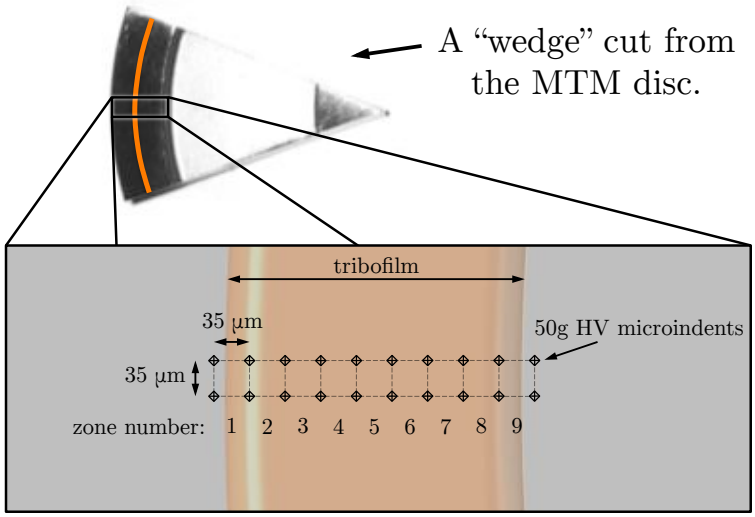


Figure 3: Schematic drawing showing microindent pattern arranged on the specimen prior to AFM experiments.

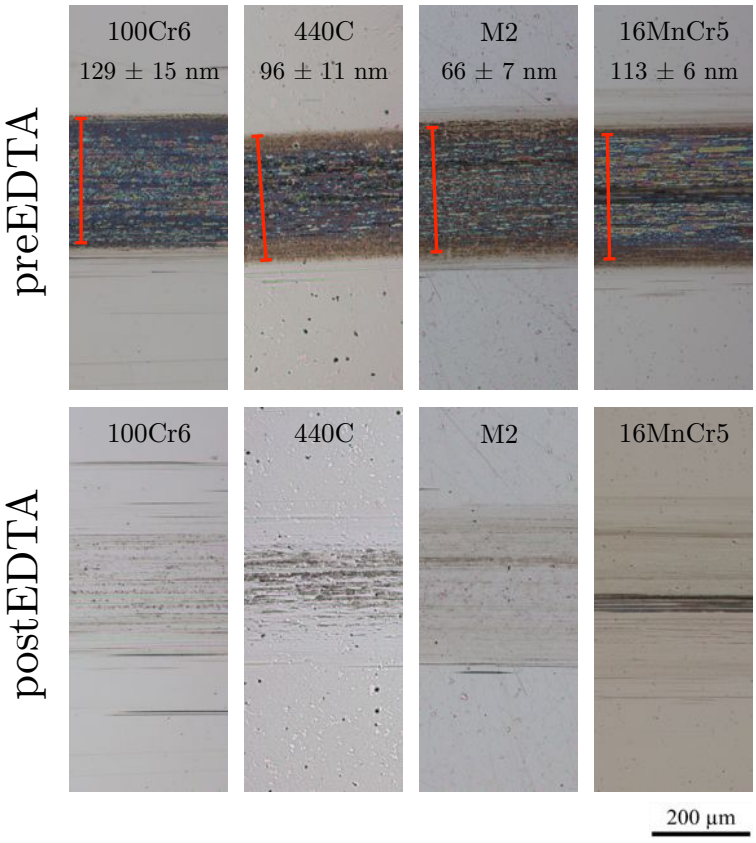


Figure 4: Optical micrographs of the MTM disc rubbing track taken before (upper part of the figure) and after removal of the tribofilm with EDTA (lower part of the figure). The orientation of the micrographs is such that the centre of the MTM disc is towards the lower part of the figure. Tribofilm thickness is indicated in preEDTA micrographs.

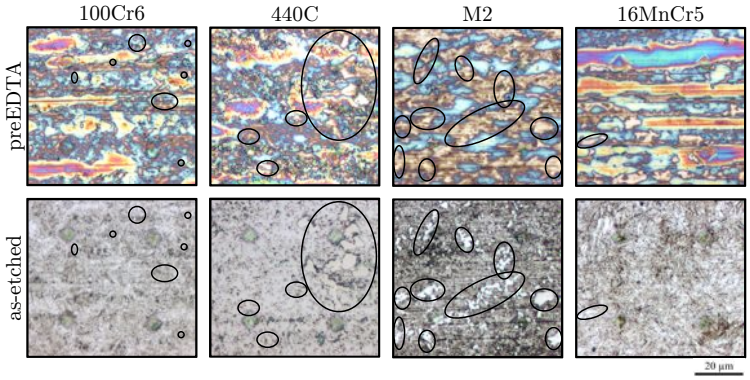


Figure 5: High magnification optical micrographs showing the tribofilm (preEDTA) and the microstructure of the underlying material (as-etched). Microindents used for relative alignment of the micrographs are visible.

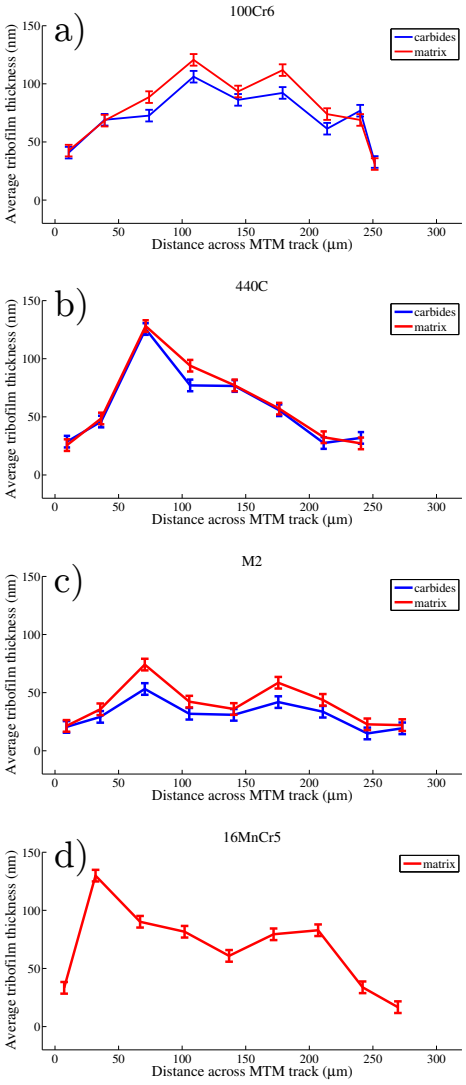


Figure 6: Average tribofilm thickness on residual carbides and matrix as a function of distance across the rubbing track.

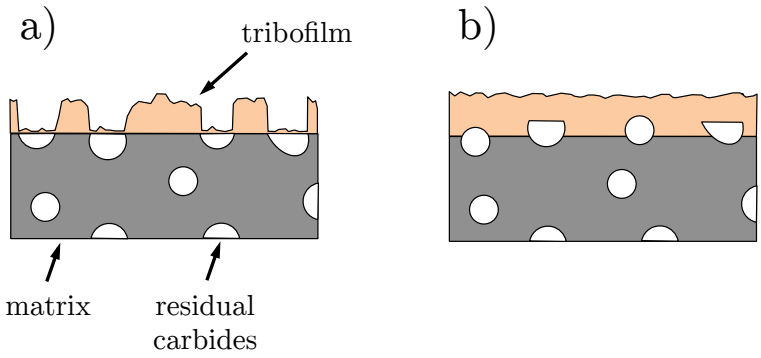


Figure 7: Two boundary cases leading to lower tribofilm thickness on residual carbides than on martensitic matrix.

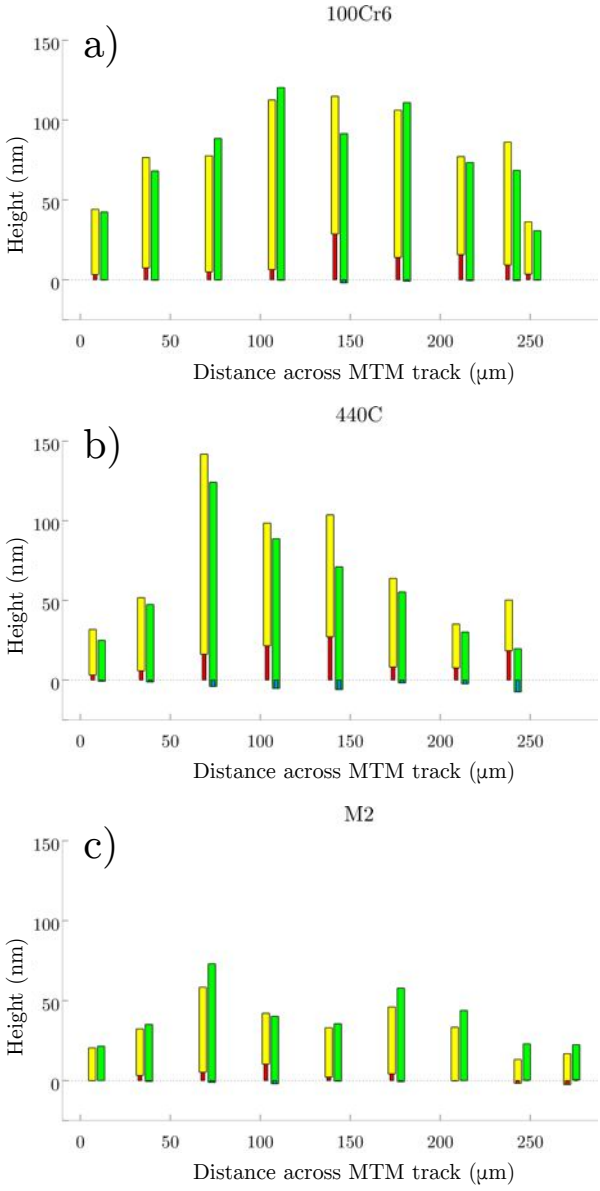


Figure 8: Plots comparing tribofilm thickness on residual carbides and martensitic matrix with carbide protrusion across the MTM disc rubbing track. Plot for 16MnCr5 is not shown as there are no residual carbides in this grade. Figure 9 provides a legend to presented data.

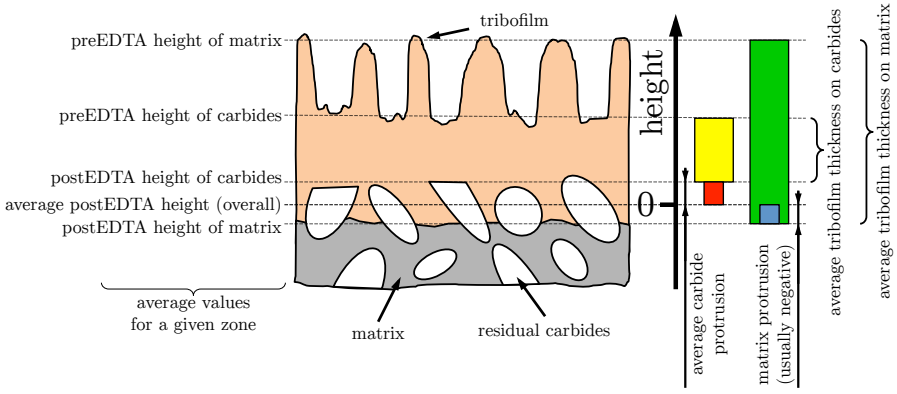


Figure 9: Schematic drawing explaining the way in which AFM data in Figure 8 is presented.

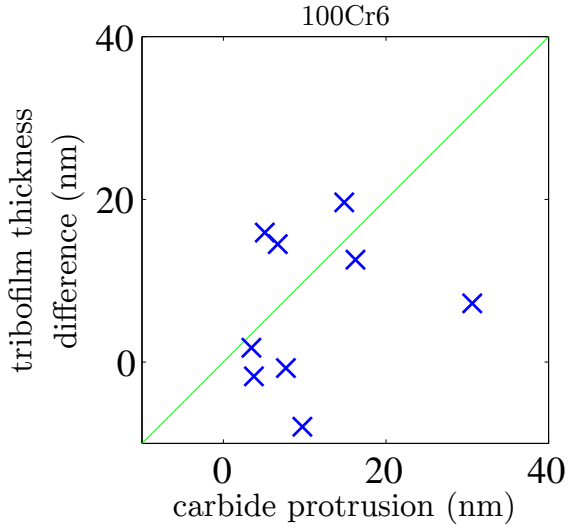


Figure 10: Difference of tribofilm thickness (matrix−carbides) as a function of carbide protrusion for 100Cr6 specimen. Each point represents a single zone. Green line corresponds to 1:1 ratio.

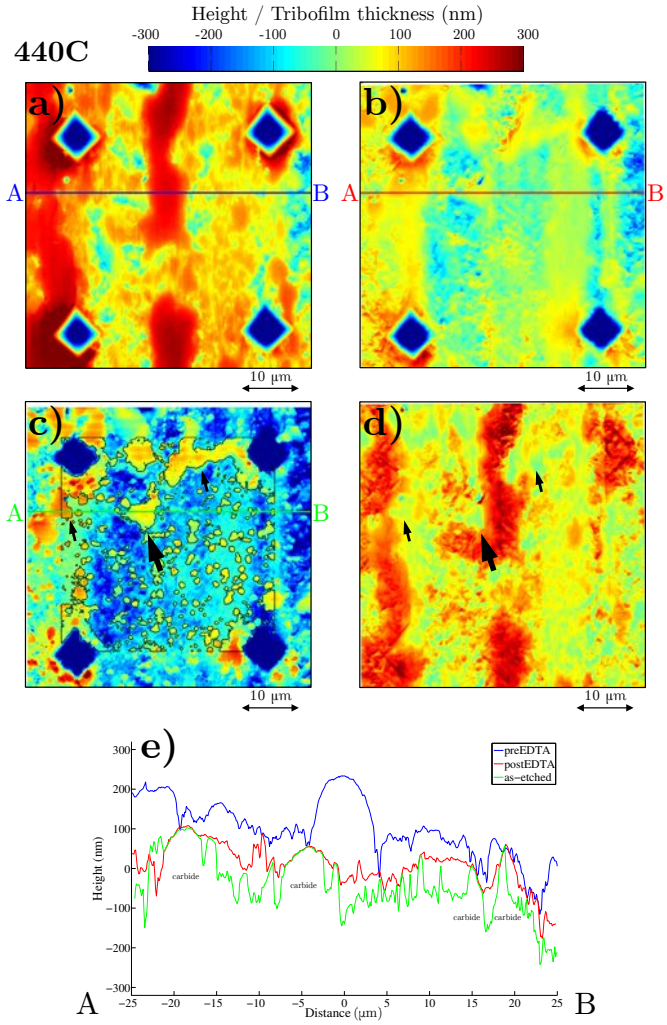


Figure 11: PreEDTA (a), postEDTA (b) and as-etched (c) AFM micrographs of zone 4 on 440C specimen. Edges of carbides in as-etched micrographs are highlighted to increase readability. Tribofilm thickness map generated with the use of the AFM method by subtracting postEDTA data from preEDTA data is shown in (d). Black arrows in as-etched micrograph and tribofilm thickness map indicate some tribofilm-free spots related with residual carbides. Profiles extracted from AFM data at marked locations are shown in e). Residual carbides related to the tribofilm free spots are marked in e).

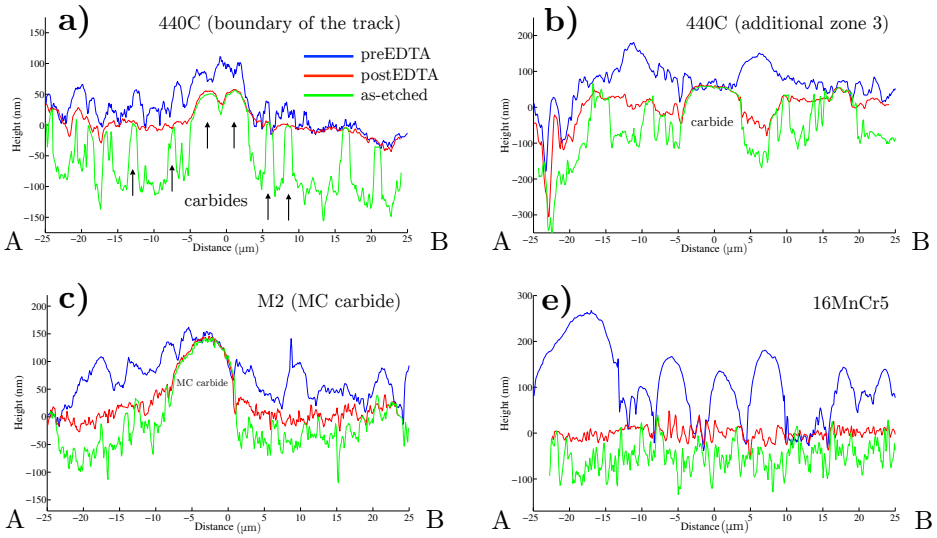


Figure 12: PreEDTA, postEDTA and as-etched profiles extracted from the AFM micrographs of a zone lying at the edge of the track of 440C steel sample (a), an additional zone 3 of the 440C specimen (b), of a large MC carbide in the M2 specimen (c) and of 16MnCr5 specimen (d). The profiles were obtained from the AFM data in the same way as shown in Figure 11 using the same cut direction. Associated AFM data used to generate profiles are shown in Figure S3a-c, Figure S5a-c, Figure S8a-c and Figure S9a-c respectively.

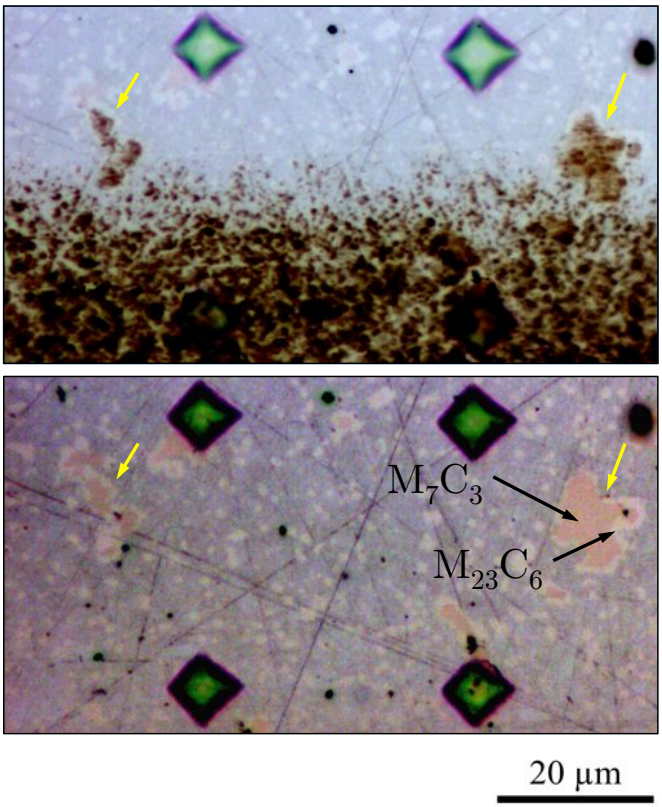


Figure 13: PreEDTA (a) and postEDTA (b) optical micrographs showing a zone laying at the boundary of the tribofilm. Brightness and contrast were digitally adjusted to highlight the preferential tribofilm formation on $M_7C_3$ carbides (marked with yellow arrows).

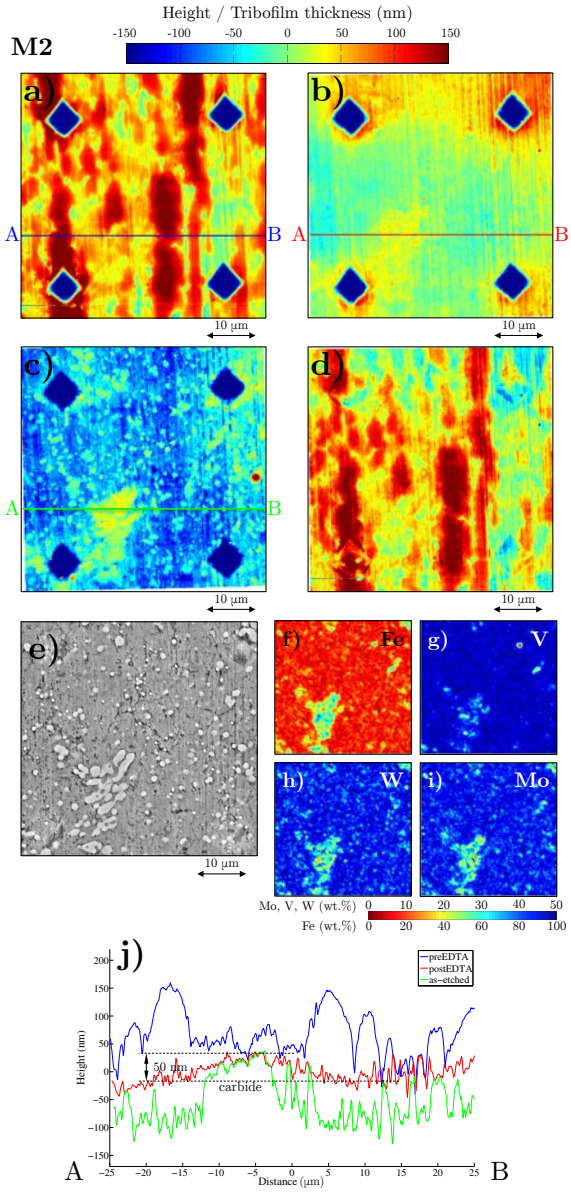


Figure 14: PreEDTA (a) and postEDTA (b) and as-etched (c) AFM micrographs of M2 specimen. Tribofilm thickness map is shown in (d). E) is the secondary electron SEM micrograph of the same region. F) - i) present the SEM/EDX maps of the same region as e) (only Fe, Mo, V and W were considered in EDX spectra quantification). Profiles extracted from AFM data at marked locations are shown in j).

Table 1: Approximate chemical composition (wt.%) of tested steel grades. Bulk composition is given for 16MnCr5.

| Grade | C | Mn | Si | Cr | Other |
|---|---|---|---|---|---|
| 100Cr6 | 1.05 | 0.3 | 0.25 | 1.5 | |
| 440C | 1.05 | 1 | 1 | 17 | Ni$\leq$0.75, Mo$\leq$0.75 |
| M2 | 0.9 | 0.3 | 0.3 | 4 | 0.3Ni, 5Mo, 2V, 6W |
| 16MnCr5 | 0.16 | 1.2 | 0.3 | 1 | |

Table 2: MTM test parameters.

| Duration | Temperature | Maximum contact pressure | Contact circle radius | Slide-roll ratio | Entrainment Speed |
|---|---|---|---|---|---|
| $t$ | $T$ | $p_{max}$ | $a$ | SRR | $v_{entr}$ |
| 12 h | 80°C | ∼1 GPa | ∼130 µm | 100% | 35 mm/s |

Table 3: Hardness and roughness of MTM samples and resultant dimensionless film thickness $\lambda$.

| Grade | Hardness (HV) | | $R_{rms}$ roughness | | |
|---|---|---|---|---|---|
| | Disc[1] | Ball[2] | Disc | Ball | $\lambda$ |
| 100Cr6 | 728 ±5 | 800-940 | 5 nm | 17 nm | 0.41 |
| 440C | 633 ±2 | 610-700 | 14 nm | 22 nm | 0.28 |
| M2 | 792 ±4 | 870-1020 | 8 nm | 41 nm | 0.18 |
| 16MnCr5 | 763 ±8 | 750-870 | 5 nm | 51 nm | 0.14 |

[1] Based on ten HV30 measurements.
[2] As reported by manufacturer.